

Optical Emission from Aspherical Core-Collapse Supernovae

Masaomi Tanaka^{*,†}, Keiichi Maeda[†], Ken'ichi Nomoto^{†,*}, Paolo A. Mazzali^{**,‡}, Nozomu Tominaga[§], Koji S. Kawabata[¶] and Takashi Hattori^{||}

^{*}*Department of Astronomy, Graduate School of Science, University of Tokyo, Tokyo, Japan;*
mTanaka@astron.s.u-tokyo.ac.jp

[†]*Institute for the Physics and Mathematics of the Universe, University of Tokyo, Kashiwa, Japan*

^{**}*Max-Planck-Institut für Astrophysik, Garching bei München, Germany*

[‡]*Istituto Nazionale di Astrofisica-OAPd, Padova, Italy*

[§]*Division of Optical and Infrared Astronomy, National Astronomical Observatory of Japan,*
Mitaka, Tokyo, Japan

[¶]*Hiroshima Astrophysical Science Center, Hiroshima University, Higashi-Hiroshima, Hiroshima,*
Japan

^{||}*Subaru Telescope, National Astronomical Observatory of Japan, Hilo, HI*

Abstract. Optical emission from supernovae (SNe) reflects physical properties of SNe, such as mass and kinetic energy of the ejecta and the ejected ^{56}Ni mass, which are closely related to the central remnants, explosion scenarios and progenitor stars of SNe. Modelling of the optical emission has been done mostly under the assumption of spherical symmetry. In this paper, we present multi-dimensional modelling of optical emission using a multi-dimensional Monte-Carlo radiative transfer code, SAMURAI (SupernovA MUlti-dimensional RAdiative transfer code). We show that all the optical observations of SN 1998bw/GRB 980425, including the light curve and optical spectra at early and late phases, are consistent with polar-viewed radiation of the aspherical explosion model. The kinetic energy, which has been estimated to be $30 - 50 \times 10^{51}$ ergs by spherical models, can be reduced to 20×10^{51} ergs. Such reduction of the kinetic energy is less effective for off-axis or less aspherical cases. As an observational test of SN asphericity, we also show our recent spectropolarimetric observations of Type Ic SN 2007gr with Subaru telescope. The data clearly indicate the difference in the distribution of the newly synthesized elements and the elements in the pre-explosion star.

Keywords: supernovae; gamma-ray bursts; radiative transfer; nucleosynthesis; polarization

PACS: 97.60.Bw; 97.10.Ex; 26.30.-k; 95.30.Gv

MODELLING OPTICAL EMISSION OF SUPERNOVAE

Optical emission from supernovae (SNe) reflects physical properties of SN ejecta. For example, the timescale (τ) of the light curve (LC) around maximum is governed by the diffusion timescale of optical photons in the SN ejecta, and thus, reflects the mass (M_{ej}) and kinetic energy (E_{K}) of the ejecta and opacity (κ) in the ejecta ($\tau \propto \kappa^{1/2} M_{\text{ej}}^{3/4} E_{\text{K}}^{-1/4}$, [1]). When the LC is powered by the radioactive decay of ^{56}Ni , the luminosity is indicative of the ejected mass of ^{56}Ni . From optical spectra, which typically show pseudo-continuum and P-Cygni profiles onto the continuum [2], we can extract the information on the elements that make absorption lines, and can measure the expansion velocity (v) from the Doppler shift of the P-Cygni absorptions ($v \propto M_{\text{ej}}^{-1/2} E_{\text{K}}^{1/2}$).

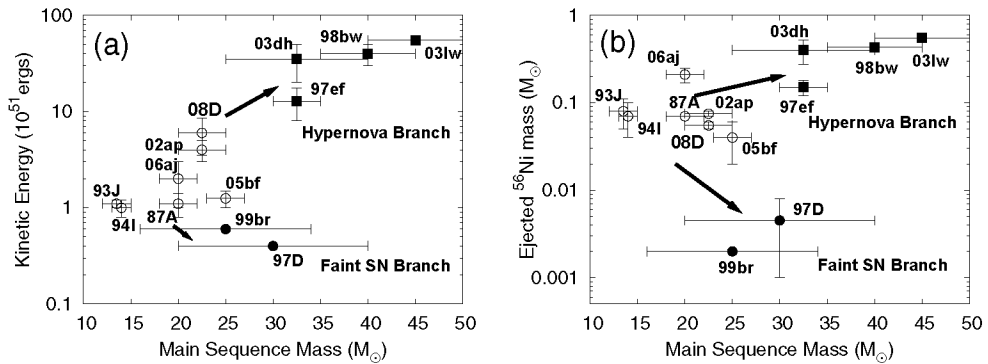


FIGURE 1. The kinetic energy (a) and the ejected ^{56}Ni mass (b) for several core-collapse SNe as a function of estimated main-sequence mass of the progenitor star (see Table 2 of Tanaka et al. [6] and references therein).

Modelling optical emission (LC and spectra) from SNe has been performed to understand the nature of the explosion, and the progenitor stars of SNe (see, e.g., [3, 4, 5, 6]). (I) By modelling the observed LC and spectra, the mass and kinetic energy can be estimated through the radiative transfer calculation (giving the value of κ and its time evolution). (II) With the estimated M_{ej} and E_{K} , the core mass prior to the explosion can be estimated. In this step, hydrodynamic and nucleosynthetic calculations are necessary to make constraints on the mass of the central remnant (see [4, 6]). (III) Main-sequence mass is estimated by the derived core mass, with the help of the evolutionary models, which predict the relation between the core mass and main-sequence mass (see Fig. 1 of Tanaka et al. [6]).

Figures 1(a) and 1(b) show the estimated kinetic energy and ejected ^{56}Ni mass for several core-collapse SNe [7, 6]. The main sequence mass for the SNe is estimated using the relation between core mass and main-sequence mass by Sugimoto & Nomoto [8], Nomoto & Hashimoto [9]. The estimated kinetic energy and the ejected ^{56}Ni mass are more diverse for larger main-sequence mass ($M_{\text{MS}} > 25 - 30M_{\odot}$) than for smaller main-sequence mass ($M_{\text{MS}} < 25 - 30M_{\odot}$). It is worth noting that this boundary corresponds to the boundary between neutron star and black hole formation (e.g., [10]).

MULTI-DIMENSIONAL RADIATIVE TRANSFER

There is increasing number of evidence for asphericity of SNe, e.g., direct imaging [11, 12], polarimetry [13, 14, 15], and spectroscopy [16, 17, 18]. However, most of the modelling works for SN emission have been done under the assumption of spherical symmetry. This could affect the estimate of the SN parameters, especially in the step (I) discussed above.

The effect of asphericity is expected to be particularly important for SNe associated with gamma-ray bursts (GRBs) since GRBs are thought to be induced by relativistic

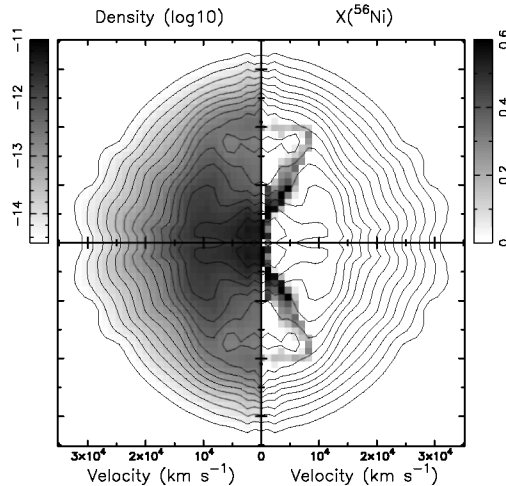


FIGURE 2. Aspherical explosion model with the kinetic energy $E_K = 20 \times 10^{51}$ ergs. *Left:* Density distribution ($\log g \text{ cm}^{-3}$) at 10 days after the explosion. The contour also shows the density. *Right:* Mass fraction of ^{56}Ni . The velocity can be used as spatial coordinate thanks to the homologous expansion ($r \propto v$).

jets (e.g., [19]). Thus, we perform multi-dimensional modelling for SNe associated with GRBs (hereafter, GRB-SNe), and see if the estimates by one-dimensional modelling are affected.

Aspherical Explosion Models

We use the results of multi-dimensional hydrodynamic and nucleosynthetic calculations for SN 1998bw by Maeda et al. [20] as input density and element distributions. Figure 2 shows the density structure (left panel and contour) and the distribution of ^{56}Ni (right panel). In the hydrodynamic model, explosion is initiated by depositing energy aspherically, with more energy in the jet direction (z-axis, defined as $\theta = 0^\circ$). As a result, ^{56}Ni is preferentially synthesized along this direction. The kinetic energy of the model is $E_K = 20 \times 10^{51}$ ergs [20, 21]. Since the original models used a He star as a progenitor [9], we simply replace the abundance of the He layer with that of the C+O layer after the nucleosynthesis calculation.

The SAMURAI Code

We have unified a SupernovA MUlti-dimensional RAdiative transfer code SAMURAI to study the detailed properties of the radiation from aspherical SNe. SAMURAI is a combination of 3D codes adopting Monte-Carlo methods to compute the bolometric LC [21, 22], and the spectra from early [23, 24] to late phases [25]¹.

The spectra are calculated as snapshots. For the early phase spectra ($\lesssim 40$ days after the explosion), a sharply defined photosphere is assumed as an inner boundary, and the results of the LC simulation are used as the luminosity at the inner boundary. For the

¹ See also [26, 27, 28, 29, 30] for other multi-dimensional radiative transfer codes for SNe.

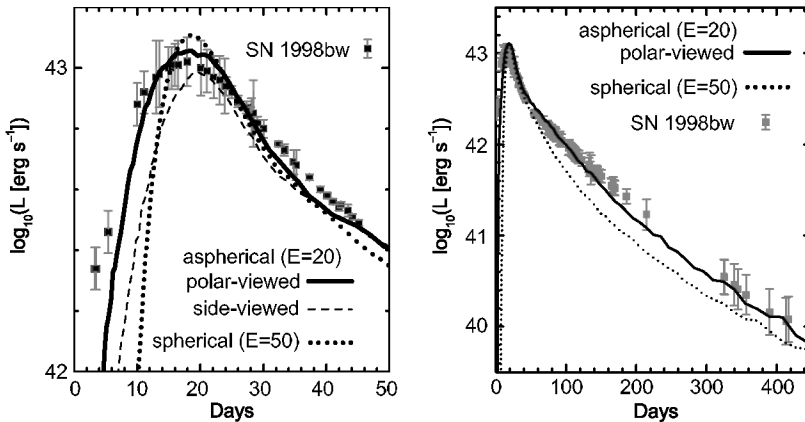


FIGURE 3. The bolometric LC of SN 1998bw (points, [37]) compared with the simulated LCs with the aspherical model with $E_K = 20 \times 10^{51}$ ergs (solid and dashed lines) and the spherical model with $E_K = 50 \times 10^{51}$ ergs (dotted line) [21]. *Left:* The LCs at early phases. The LC of the polar-viewed ($\theta = 0^\circ$) case rises earlier than that of the side-viewed ($\theta = 90^\circ$) case. *Right:* The LCs until late phases. The LC of the spherical model fades faster than the observed LC.

late phase spectra ($\gtrsim 200$ days after the explosion), the energy deposition by radioactive decay of ^{56}Ni and ^{56}Co derived in the LC simulation is used as input. The local physical processes to determine the ionization and excitation states are the same as in the previous 1D codes [31, 32, 34, 33].

Bolometric Light Curves

Maeda et al. [21] computed bolometric LCs using the aspherical explosion model described above. Under the spherical symmetry, a model with $E_K = 30 - 50 \times 10^{51}$ ergs reproduce the observed LC and spectra at early phases [35, 4, 36]. However, this model predicts a faster decline at later phases (dotted line in the right panel of Figure 3) because of the insufficient trapping of γ -rays.

This problem can be solved by aspherical models with a polar view. In the aspherical model, a lower kinetic energy is assumed ($E_K = 20 \times 10^{51}$ ergs), which allows sufficient trapping of γ -rays at late times. One might expect that the timescale of the LC around maximum would become longer due to the expected longer timescale for photon diffusion. However, in the polar-viewed case, since the distribution of ^{56}Ni is extended (Fig. 2), the timescale of the LC is also reproduced (solid line in the left panel of Fig. 3).

Optical Spectra

We test the aspherical model against the observed spectra by performing multi-dimensional radiative transfer simulations [24]. Figure 4 shows the observed spectra at 18 (left panel) and 30 (right panel) days after the explosion, compared with synthetic spectra.

If the explosion is observed from the polar direction (black solid line in Fig. 4), which is consistent with the detection of GRB, the observed high velocities of the Si and Fe lines can be explained. The most distinguishing features are Fe lines at 30 days after the explosion. For the side-viewed case (dashed line), there are two strong peaks near

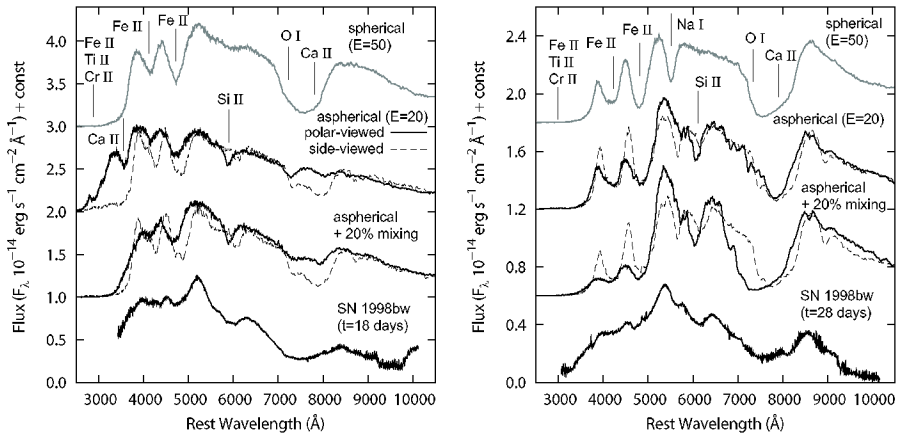


FIGURE 4. *Left:* The observed spectrum of SN 1998bw at 18 days after the explosion compared with the synthetic spectra computed with the spherical with $E_K = 50 \times 10^{51}$ ergs (gray), the two aspherical models with $E_K = 50 \times 10^{51}$ ergs without/with additional mixing. For aspherical models, the solid and dashed lines show the spectra viewed from polar ($\theta = 0^\circ$) and equatorial ($\theta = 90^\circ$) direction, respectively. The synthetic spectra are shifted by $3.0, 2.0, 1.0 \times 10^{-14}$ from top to bottom. *Right:* Same as the left panel but at 30 days after the explosion. The synthetic spectra are shifted by $1.8, 1.2, 0.6 \times 10^{-14}$ from top to bottom.

4000 and 4500 Å, while these are not seen in the polar-viewed case (solid line). The suppression of the peaks is similarly seen in the spectrum of SN 1998bw. This is the effect of the extended Fe distribution around the pole.

The strengths of the lines depend on both (a) the element distribution and (b) ionization states in the ejecta. At earlier epochs (left panel of Fig. 4), the effect of (b) is remarkable. Since ^{56}Ni is distributed around the pole, the ejecta temperature is higher for the polar region. This leads to overionization of Fe, Ca, and O contained in the pre-explosion star, and makes the absorption lines of Fe II, Ca II and O I weaker in polar-viewed spectrum. At later phases (right panel), this is compensated by the effect of (a) since heavy elements are synthesized around the pole.

In the polar-viewed spectrum, the Ca II line (IR triplet, marked near 7800 Å) is weaker than the observed feature. This may require additional mixing. In the models shown in Fig. 4, 20 % of synthesized material is assumed to be mixed to the outermost layer.

IMPLICATIONS OF MULTI-DIMENSIONAL MODELLING

We have presented the simulations of optical emission from jet-like aspherical explosion. The emergent LC and spectra are different depending on the viewing angles, which reflect both aspherical abundance distributions and anisotropic ionization states.

The LC study shows that the total kinetic energy, which is estimated to be $30 - 50 \times 10^{51}$ ergs by spherical models, can be reduced to 20×10^{51} ergs by the polar-viewed aspherical model. The smaller kinetic energy is also acceptable for the spectra although

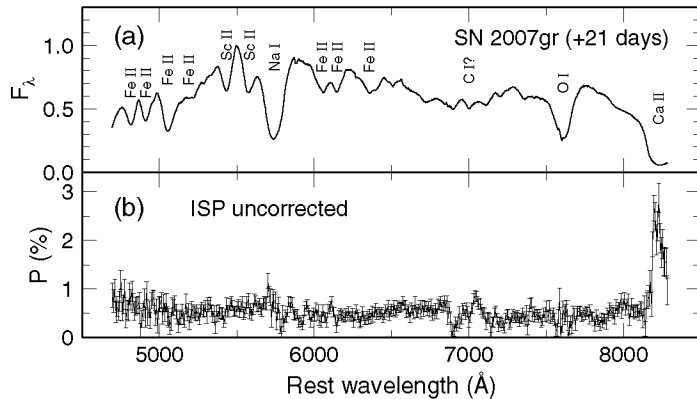


FIGURE 5. (a) Spectrum of SN 2007gr at 21 days after the maximum brightness. Flux is written in $10^{-14} \text{erg s}^{-1} \text{cm}^{-2} \text{\AA}^{-1}$. Strong lines are marked. (b) Polarization spectrum of SN 2007gr. Interstellar polarization (ISP) is not corrected. Depending on the choice of ISP, the continuum polarization could be 0-0.5 %. The high polarization level at Ca II line is independent on the choice of the ISP. See Tanaka et al. [43] for more details.

the agreement is not perfect. It should be noted that the higher kinetic energy than the canonical SNe ($E_K \sim 10^{51} \text{erg}$) is still required for GRB-SNe.

For both LC and spectra, the extended distribution of synthesized elements in the polar direction causes important effects (rapid rise of the LC and line broadening in the spectra). Thus, the reduction of the kinetic energy is the most effective in the polar-viewed case, while there is little effect for the side-viewed case. Also, since normal Type Ib/c SNe are thought to be less aspherical than GRB-SNe [17], the effect of asphericity on the estimate of the kinetic energy may be smaller for normal Type Ib/c SNe.

The simulations enable us to predict the radiation from off-axis supernovae. The LC viewed off-axis rises more slowly than that of on-axis, and its maximum brightness is slightly fainter (Fig. 3). At early phases, the spectra viewed off-axis show (1) a slightly lower absorption velocity, (2) stronger peaks around 4000 and 4500 \AA (narrower absorption of Fe) and (3) a stronger Na I $\lambda 5890$ line. At later phases, off-axis supernovae would show double-peaked [O I] emission profile [16, 17, 18].

PROBING ASPHERICITY BY SPECTROPOLARIMETRY

Optical emission from aspherical supernovae differ depending on the directions. It is, however, difficult to directly study asphericity of the explosion only from the LC and early phase spectra because we cannot specify the viewing-angle in most cases (except for GRB-SNe). One might use late phase spectra, which show the characteristic line profiles to identify the viewing angle and to study the asphericity of the explosion [16, 17, 18].

Polarization at early phases is one of the most direct method to study the asphericity

of extragalactic SNe since the polarization would not be detected from spherically symmetric ejecta [38, 39]. Especially, spectropolarimetry is useful because the polarization across the P-Cygni profile can give the information on the distribution of the elements. Spectropolarimetric studies have clarified the asymmetric nature of core-collapse SNe in detail [40, 41, 13, 42, 15, 14].

We performed spectropolarimetric observations of Type Ic SN 2007gr [43] with the 8.2 m Subaru telescope equipped with the Faint Object Camera and Spectrograph (FOCAS, [44]). SN 2007gr is an unique Type Ic SN since it shows the absorption features of C lines [45]. Figure 5 shows the flux/polarization spectrum taken at 21 days after the maximum brightness. Interstellar polarization (ISP) is not corrected in the polarization spectrum.

A high polarization level as high as $\sim 3\%$ is detected in the Ca II line, while such a high polarization is not detected in the similarly strong Na I and O I lines. This clearly indicates the distributions of Ca II and Na I/O I are different. Within the uncertainty of ISP, the continuum polarization can be 0-0.5 %.

Considering our multi-dimensional radiative transfer simulations, non-spherical line formation can be caused by the following two reasons; (a) aspherical element distributions or (b) anisotropic ionization states (see also [46]). However, in the case of (b), Ca II, Na I, and O I ions will be similarly enhanced, and show a similar polarization level at these lines, which is not consistent with the observed features in SN 2007gr. Thus, for SN 2007gr, different polarization levels seen in these lines reflects the element distributions. It proves that there is a difference in the distribution of newly synthesized elements (Ca) and that of the elements in the pre-explosion star (Na and O). For more quantitative discussion, polarization modelling is required [26, 47].

SUMMARY

Optical emission of SNe has been modelled to study the properties of the SN ejecta, central remnants and progenitor stars. Although there is increasing number of evidence for asphericity of SNe, most of the modelling works have assumed spherical symmetry. We have developed multi-dimensional radiative transfer code SAMURAI. The code has been utilized to model the optical emission from GRB-SNe. If the explosion is observed from the polar direction, the estimate of the kinetic energy can be reduced because of the extended distribution of synthesized elements around the pole. This effect is less significant in side-viewed or less aspherical cases. Spectropolarimetry is a powerful method to study the distribution of elements in SN ejecta. Our observation shows the different distribution of newly synthesized elements and elements in the pre-explosion star.

ACKNOWLEDGMENTS

M.T. is supported through the JSPS (Japan Society for the Promotion of Science) Research Fellowship for Young Scientists.

REFERENCES

1. Arnett, W. D., *ApJ* **253**, 785 (1982)
2. Filippenko, A. V., *ARA&A* **35**, 309 (1997)
3. Mazzali, P. A., Iwamoto, K., & Nomoto, K., *ApJ* **545**, 407 (2000)
4. Nakamura, T., Mazzali, P. A., Nomoto, K., & Iwamoto, K., *ApJ* **550**, 991 (2001)
5. Sauer, T., Mazzali, P. A., Deng, J., Valenti, S., Nomoto, K., & Filippenko, A. V., *MNRAS* **369**, 1939 (2006)
6. Tanaka, M., et al., *ApJ*, in press (2009), arXiv:0807.1674
7. Nomoto, K., Tominaga, N., Tanaka, M., Maeda, K., Suzuki, T., Deng, J. S., & Mazzali, P. A., in *SWIFT and GRBs: Unveiling the Relativistic Universe, II Nuovo Cimento* **121**, 1207 (2007), astro-ph/0702472
8. Sugimoto, D., & Nomoto, K., *Space Science Reviews* **25**, 155 (1980)
9. Nomoto, K., & Hashimoto, M., *Phys. Rep.* **163**, 13 (1988)
10. Heger, A., Fryer, C. L., Woosley, S. E., Langer, N., & Hartmann, D. H., *ApJ* **591**, 288 (2003)
11. Wang, L., et al., *ApJ* **579**, 671 (2002)
12. Hwang, U., et al., *ApJ* **615**, L117 (2004)
13. Wang, L., Howell, D. A., Höflich, P., & Wheeler, J. C., *ApJ* **550**, 1030 (2001)
14. Kawabata, K. S., et al., *ApJ* **580**, L39 (2002)
15. Leonard, D. C., et al., *Nature* **440**, 505 (2006)
16. Mazzali, P. A., et al., *Science* **308**, 1284 (2005)
17. Maeda, K., et al., *Science* **319**, 1220 (2008)
18. Modjaz, M., Kirshner, R. P., Blondin, S., Challis, P., & Matheson, T., *ApJ* **687**, L9 (2008)
19. Piran, T., *Rev. Mod. Phys.* **76**, 1143 (2005)
20. Maeda, K., Nakamura, T., Nomoto, K., Mazzali, P. A., Patat, F., & Hachisu, I., *ApJ* **565**, 405 (2002)
21. Maeda, K., Mazzali, P. A., & Nomoto, K., *ApJ* **645**, 1331 (2006)
22. Maeda, K., *ApJ* **644**, 385 (2006)
23. Tanaka, M., Mazzali, P. A., Maeda, K., & Nomoto, K., *ApJ* **645**, 470 (2006)
24. Tanaka, M., Maeda, K., Mazzali, P. A., & Nomoto, K., *ApJ* **668**, L19 (2007)
25. Maeda, K., Nomoto, K., Mazzali, P. A., & Deng, J., *ApJ* **640**, 854 (2006)
26. Höflich, P., Wheeler, J. C., Hines, D. C., & Trammell, S. R., *ApJ* **459**, 307 (1996)
27. Höflich, P., Wheeler, J. C., & Wang, L., *ApJ* **521**, 179 (1999)
28. Thomas, R. C., Kasen, D., Branch, D., & Baron, E., *ApJ* **567**, 1037 (2002)
29. Kasen, D., Thomas, R. C., & Nugent, P., *ApJ* **610**, 876 (2004)
30. Sim, S. A., *MNRAS* **375**, 154 (2007)
31. Mazzali, P. A. & Lucy, L. B., *A&A* **279**, 447 (1993)
32. Mazzali, P. A., *A&A* **363**, 705 (2000)
33. Mazzali, P. A., Nomoto, K., Patat, F., & Maeda, K., *ApJ* **559**, 1047 (2001)
34. Ruiz-Lapuente, P., & Lucy, L. B., *ApJ* **400**, 127 (1992)
35. Iwamoto, K., et al., *Nature* **395**, 672 (1998)
36. Maeda, K., Mazzali, P. A., Deng, J., Nomoto, K., Yoshii, Y., Tomita, H., Kobayashi, Y., *ApJ* **593**, 931 (2003)
37. Patat, F., et al., *ApJ* **555**, 900 (2001)
38. Shapiro, P. R., & Sutherland, P. G., *ApJ* **263**, 902 (1982)
39. Höflich, P., *A&A* **246**, 481 (1991)
40. Cropper, M., Bailey, J., McCowage, J., Cannon, R. D., & Couch, W. J., *MNRAS* **231**, 695 (1988)
41. Trammell, S. R., Hines, D. C., & Wheeler, J. C., *ApJ* **414**, L21 (1993)
42. Leonard, D. C., Filippenko, A. V., Ardila, D. R., & Brotherton, M. S., *ApJ* **553**, 861 (2001)
43. Tanaka, M., Kawabata, K. S., Maeda, K., Hattori, T., & Nomoto, K., *ApJ* **689**, 1191 (2008)
44. Kashikawa, N., et al., *PASJ* **54**, 819 (2002)
45. Valenti, S., et al., *ApJ* **673**, L155 (2008)
46. Höflich, P., Khokhlov, A., & Wang, L., in *AIP Conf. Proc.* 586, 20th Texas Symposium on Relativistic Astrophysics, ed. J. C. Wheeler & H. Martel (New York: AIP), 459 (2001)
47. Kasen, D., et al., *ApJ* **593**, 788 (2003)